Ben-Gurion University of the Negev

Faculty of Engineering Sciences

Department of Materials Engineering

CuS Nanoparticles:
Automatic Size Calculation

By: Ofir Friedman

Lecturer: Prof. Amit Kohn

Course: Image Processing for Materials Science Applications

January 2015

Table of Contents

List of Figures

List of Tables

1 Introduction

Synthesis of Copper sulfide (CuS) nanoparticles has been studied intensely over the last decade, due to their electrical and optical properties. CuS nanoparticles demonstrate increased absorbance in the shortwave infrared range (SWIR) wavelengths due to localized surface plasmon resonance (LSPR). The absorbance intensity and wavelength are dependent on shape and size of these nanoparticles, and can be further controlled by varying the stoichiometric ratio and height to width ratio of the nanoparticles. A large variety of shapes and sizes has been reported: cuboctahedrons, nanotubes, nanoflake and more[1-5]. CuS nanoparticles can be synthesized on various substrates using a variety of methods.[6-14] LSPR manifests as a significant increase in optical absorption at specific wavelengths, and makes the nanoparticles a potential material for applications in various fields, such as: Dyes in solar cells[15], thin films application[16] and quantum dots[17].

LSPR is an optical phenomenon that is intensively researched and applied in many fields such as electronics, optical sensing, data storage, light generation and more[18-22]. LSPR is created from interaction between incident light and electrons in the conduction band. As a result of this interaction coherent localized plasmon oscillations are created. The LSPR frequency in a nanoscale material is strongly dependent on the nanoparticles composition, shape, size distance between particles and dielectric environment. The LSPR is well known in metallic nanoparticles. Once confinement is achieved, electron bands become discrete and plasmon resonance will scale accordingly. An important aspect of the LSPR is the size effect. The surface size of the nanoparticles directly affects the absorption cross-section and scattering cross-section of scatter. Absorption is dominant in nanoparticles that are smaller than 20nm. As size increases the scattering cross-section increases accordingly and the absorption effect deteriorates.

Covellite is a unique nanoparticle in aspect of LSPR due to the fact that it is not a classical metallic nanoparticle but semi-metallic. The LSPR is explained by the presence of one third of a hole for each chemical formula unit of CuS.[23-26] The covellite nanoparticles synthesized in this work can be linked to ultrathin nanodisk shape that possesses in-plane and out-of-plane dipoles as can be seen in Figure 1.1. LSPR in those nanoparticles can be modulated by controlling the thickness to width ratio.[21] Thus, control over this ratio has drastic implications.

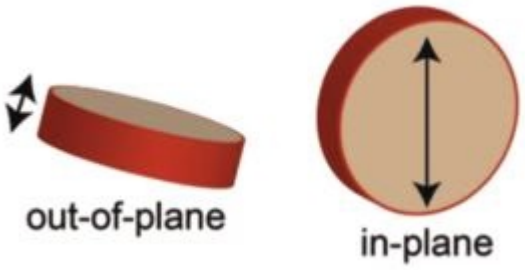

Figure 1.1: *In plane and out of plane dipole directions in ultrathin nanodisks.*[20]

In this work an automatic code for collection of the CuS nanoparticles thickness and width is suggested. The code is written in Matlab and uses its advanced image processing tools. Bright field TEM images were produced using Ilse Katz Institute for Nanoscale Science & Technology TEM JEM-1230 (T-12). The images were converted from DigitalMicrograph '.dm' format to '.TIF' files. Graphical and statistical analyze of the '.TIF' files was conducted using Origin and Statistica software.

2 Assumptions

A set of basic assumptions was determined for particles detection, filtering and calibration. Firstly, Particles are parallel to the plain. Particles that did not assembled into the arrays morphology and are spread as perpendicular single particles will be considered as noise. Under the same demand multi-nanoparticles clusters and none parallel particles will also be disregard. Secondly the magnification range in which DigitalMicrograph software generates a scale bar of 20nm or 50nm was set to be the working magnification range of the program. This assumption is essential due to lack of particles and short range orders at the background of the image that are problematic to disregard. Alongside to the high magnification, 200nm scale bars magnifications lack the details required for the image processing mechanisms. Finally, the automatically generated scale bar at the bottom of the image is required to be clear of particles for pixel to nm conversion factor.

3 Image Processing

The image process is consists of two main stages. The first stage is to distinguish the particles modifying an identical image to the original one. The second stage is histogram analysis.

(a) (b)

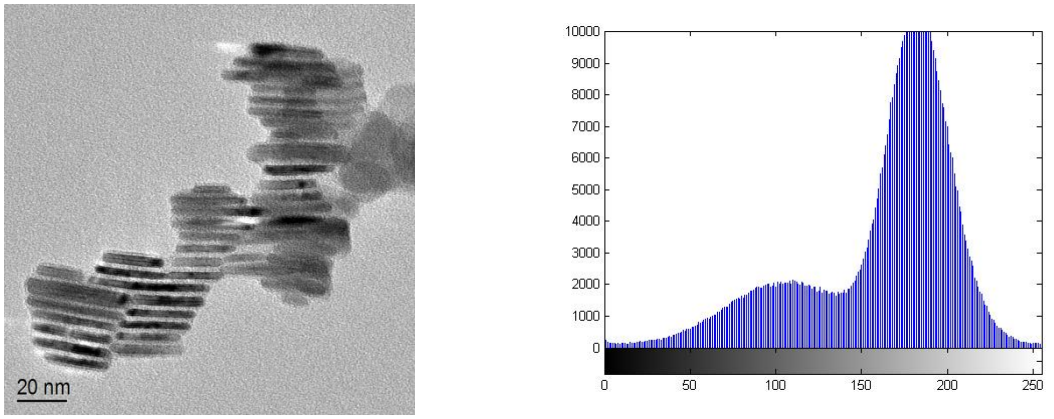

Figure 3.1: *The original images as taken from the T-12. (a)Bright field (BF) TEM image of ODA coated CuS nanoparticles. (b) Histogram of the original image.*

Figure 3.1 presents the original image and histogram. By observing the image in Figure 3.1a and considering the assumptions mentioned in the previous chapter we would expect the program to detect a group of particles in the lower left corner of the image and a few in the center and right side. In addition all other none parallel particles are expected to be ignored as background.

(a) (b)

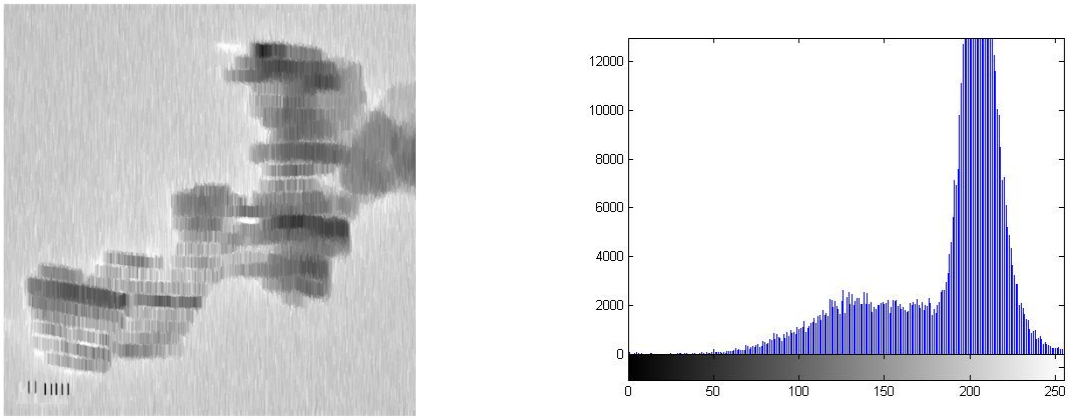

Figure 3.2: *"imclose" function applied on the original image. (a) Modified BF TEM image present the new line appearance. (b) Modified histogram of the image.*

The first stage of distinguishing the CuS nanoparticles begins with the function imclose:

$$(1)\,imclose((background, strel('line', 20, angleofScan)));$$

Code (1) represents the function call and parameters. “background” is the copy of the image in Figure 3.1a and the object “strel” define the image modification rules: ‘line’ represent the shape and 20 is the amount of pixels to be effected by this shape. “angleofScan” is a variable controlling the angle of the line and will be discussed in the automation chapter. Figure 3.3 illustrate the area of effect of code (1).

Figure 3.3: *“imclose” function set to 'line' for 20 pixels area of effect.*

As a result of the code two orders takes place. The first one is expansion of the white color (Dilation) and the second one is expansion of the black (Erosion). Consequently, the image contains random lines of black and white: The background of the image remains without order and the parallel particles have the most consistent line structure as can be seen in Figure 3.2a.

(a) (b)

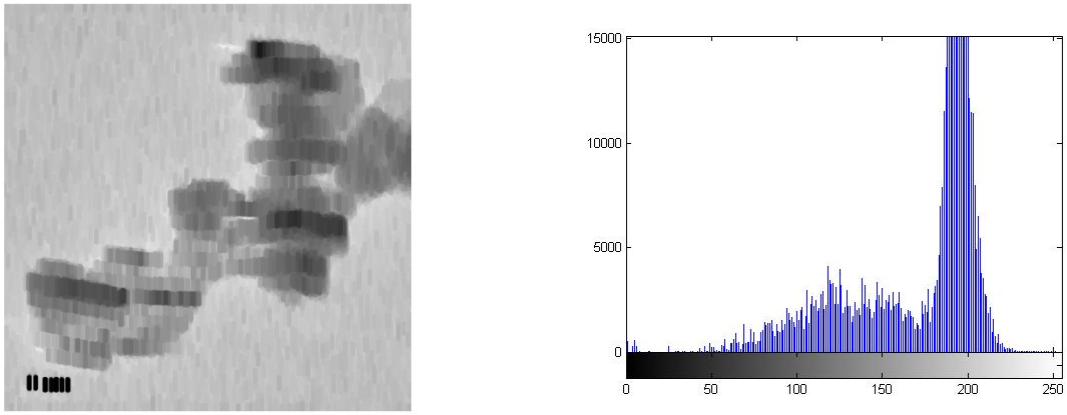

Figure 3.4: *“imrode” function applied on the original image. (a) Modified BF TEM image present the new line appearance. (b) Modified histogram of the image.*

The modification made to the image by the order (1) is significant but is not sufficient for the nanoparticles to be properly identified. Therefor code (2) is necessary:

$$(2)\,imrode((background, strel('disk', 5, angleofScan)));$$

The function “imrode” conduct erosion which means expansion of the black, as previously explained. Figure 3.5 illustrate the area of effect of code (2): a disk shape replaces the line and area of 5 pixels becomes black.

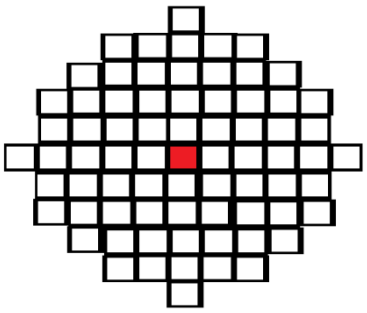

Figure 3.5: *“imrode” function set to 'Disk' for 5 pixels area of effect.*

The effect of code line (2) is merging of the black line only where they are close to each other, a property true only to parallel particles. Other areas of the image will have no significant effect due to this action. The unified black lines can be clearly seen in Figure 3.4.

(a)

(b)

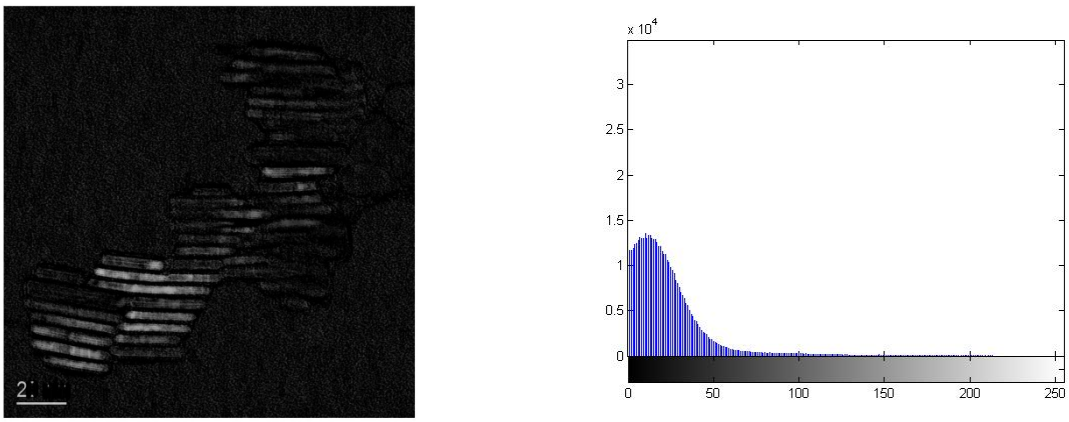

Figure 3.6: *A new image generated by reduction of the original image “I” from the modified image “background”. (a) Modified BF TEM image present the new image. (b) Modified histogram of the image.*

The end of the first stage is marked by the following code:

(3) $I2 = background - I;$

By applying code (3) a new image is created. This image is the difference between the modified image to the original: Figure 3.6b is the subtraction of Figure 3.1 from Figure 3.4b. The outcome of this mathematical action can be observed in Figure 3.6a. In this image the parallel nanoparticles are significantly brighter than the background and all none parallel objects.

(a) (b)

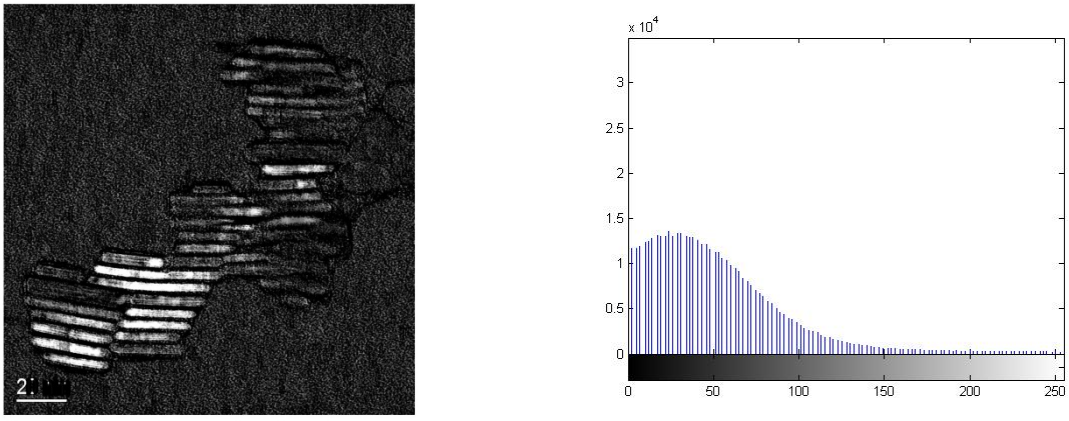

Figure 3.7: *"imadjust" function applied on the image I2. (a) Modified BF TEM image shows an improved contrast of the white area against the black area. (b) Stretched histogram of the image.*

In the second stage of the image processing is analyzes of the modified data gained from the first stage. The relevant data is located as the white edge of the histogram. Therefore, an extraction of it is required. Firstly, the histogram is stretched by code (4):

(4)*imadjust*(*I*2);

The stretching of the histogram can be clearly observed when comparing Figure 3.6b to Figure 3.7b. The histogram in Figure 3.6b is stretched between 0 to ~210 leaving approximately ~45 empty columns. On the contrary, the Figure 3.7b is stretched throughout the whole histogram. Comparison between Figure 3.7a and Figure 3.6a reveals a much clearer presentation of the nanoparticles.

As the histogram was stretched (Figure 3.7) a separation of the image to black and white pixels was required. The threshold from which the image is separated to black and white pixels was conducted by Otus's method.[27] Nobuyuki Otus suggested a simple and efficient method of separation as can be seen in code line (5) and (6):

(5)for T=0:1:255

(6)$\sigma_T^2 = \sigma_W^2 + \sigma_B^2$;

T is the counter that scans the histogram on the x axis, as can be seen in code line (5) and Figure 3.8 The method's purpose is to find the value T in which the squared sum of the variances (code line (6)) is minimal. Once the 256 round scan is completed the threshold is decided and the image can be transformed to black & white. This method is required due to complicated histograms that cannot be simply separated into black and white, as can be seen in Figure 3.8.

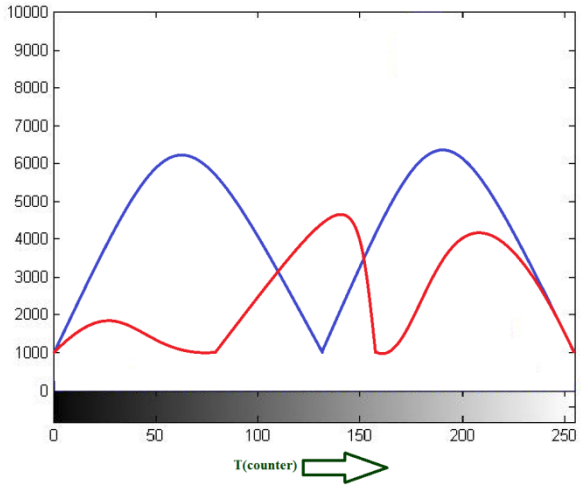

Figure 3.8: *Simple and complicated theoretical histograms. While the blue histogram is simple to analyze for black and white pixels separation the red histogram is complicated and the threshold cannot be simply guessed. The green arrow represents the T counter of the Otus's method.*

(a) (b)

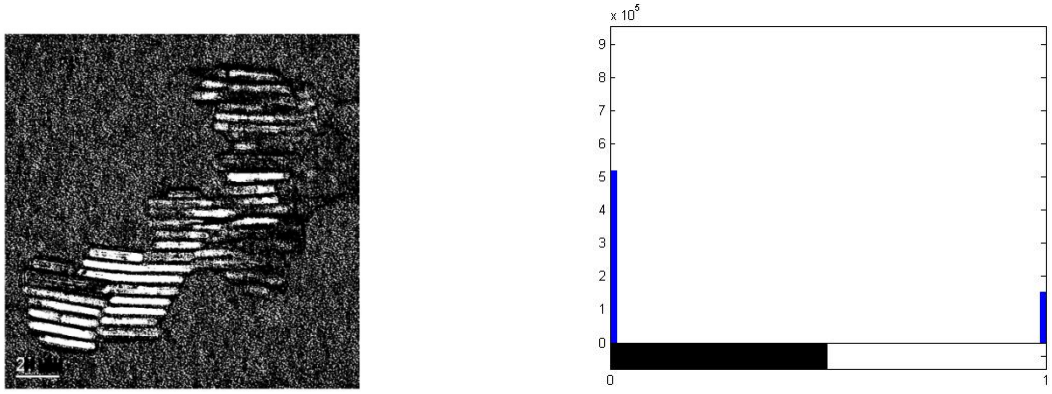

Figure 3.9: *Otus's method suggested by Nobuyuki Otus in 1979. A method of finding the gray-scale histogram threshold. The threshold separates the bright pixels from the dark pixels and allows the creation of black & white image.* [27] *(a) Modified BF TEM image transformed into Black & white pixels only. (b) The histogram of the new black & white image.*

The result of applying Otus's method on Figure 3.7 is presented in Figure 3.9. The different between Figure 3.7a to Figure 3.9a is the loss of the gray-scale and the formation of a black & white image. This change can clearly be seen in Figure 3.9b. By conducting this modification the nanoparticles that are required for analyses are completely white and some none relevant objects are also white. This problem requires one last command to be executed.

(a)

(b)

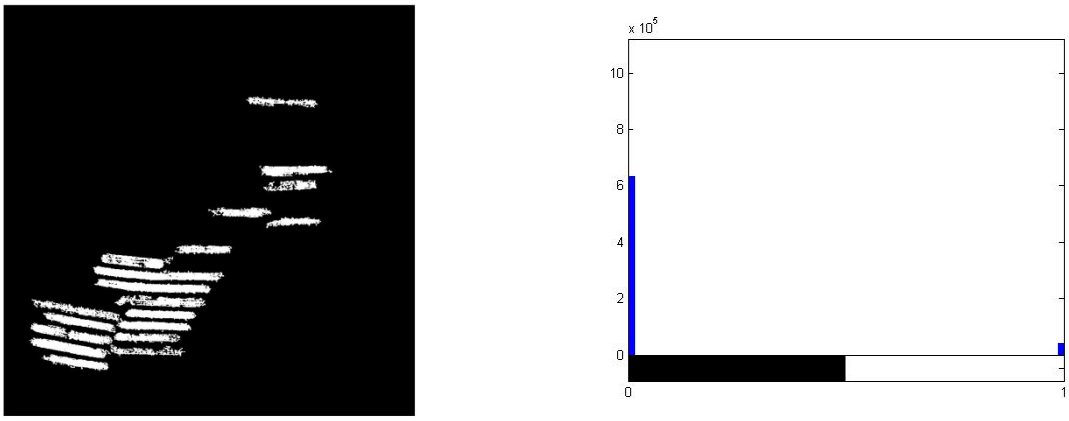

Figure 3.10: *matlab's "bwareadopen" function effect on the image. (a) Modified BF TEM image shows background noise removal. (b) A black & white histogram in which the white pixels count is further reduced by the loss of the background noise.*

The last task left for the image to be ready for data extraction and processing is the removal of the background noise. This assignment was conducted by applying the function "bwareaopen" as can be seen in code line (7):

(7)bwareaopen(bw,SmallestObjectToRemove);

The function presented in code line (7) removes particles that are smaller than a specific amount of pixels from the image. The current image name is "bw" and the noise removal threshold is "SmallestObjectToRemove". This threshold will be discussed in the Automation chapter.

Figure 3.10 is the outcome of the noise removal function. It can be seen in Figure 3.10a that only the relevant nanoparticles are white while all other irrelevant pixels are black. Figure 3.10b represents a reduction of the white column as the noise is removed. The remains of this column are the nanoparticles pixels that need to be analyzed.

By conducting the above image processing steps only relevant white pixels left. Further Analyze of the data was conducted using two more functions. Firstly, the function

“bwconncomp” was applied for detection of the white objects under a black background creation of object items in Matlab containing a list of pixels position on the image map to each white object. Secondly, a function called “regionprops” can analyze the objects list created by the “bwconncomp” function. “regionprops” was used to generate a list to objects containing 2 cells: “Major Axis Length” and “Minor Axis Length”. The list of objects was generated in pixel values and converted to nanometer scale by an auxiliary function that produce the appropriate conversion factor from the scale size given by the user and the scale bar length.

4 Automation

While Chapter 3 dealt with the image processing core mechanism this chapter deals with the automation of the program. The automation of a program is the most complicated part of the work as numerous images with different characterization needed to be processed properly and produce reliable results.

The Automation mechanism is relaying on several dynamic algorithms that take place during and after the image processing. The first add-on of automation is a loop that sets the “angleofScan”, as can be seen in code (1). “angleofScan” is a counter that runs from zero to 180 in intervals of 20. The meaning of this variable is the angle of the line created to in-light the nanoparticles. Therefore, only parallel objects to the scan will be detected and an active angle scan is required. The angle is set to scan value between zero to 180 due to the fact that any scan after 180 is a repeat of an already conducted scan at the opposite angle. In addition, an interval of 20 degrees was chosen by experiments. On the one hand, smaller intervals will produce more and the computer processing time will dramatically increase. On the other hand, as the interval increases more objects will be missed. In addition, Code line (8) and (9) were added in order to prevent repetition of objects as scan takes place several times and some nanoparticles may be detected more than once:

$$(8)\text{FamiliarObject} = \text{sum}\left(\frac{\text{FinalImage}(\text{cell2mat}(\text{cc}(\text{compareCounter}).\text{PixelIdxList}(\text{NewObjectNumber}))) >= 1)}{\text{length}(\text{cell2mat}(\text{cc}(\text{compareCounter}).\text{PixelIdxList}(\text{NewObjectNumber}))}\right)\times 100;$$

$$(9)\text{isequal}(\text{cc}(\text{compareCounter}).\text{PixelIdxList}(\text{NewObjectNumber}), \text{ccFinal}.\text{PixelIdxList}(\text{FinalObjectNumber})) \;||\; \text{FamiliarObject} >= 90$$

Code (8) compares each pixel of the newly found object with an object from the generated database of object and returns a percentage of familiarity. The code repeats itself for all objects in the database. The percentage of familiarity is defined in code (9). If the new object is similar to any other object in the database at up to 90% familiarity it will be disregarded.

Furthermore, a second variable was added to the program that handles the noise reduction factor. This variable is called “SmallestObjectToRemove” as can be seen in code (7). Similarly to the “angleofScan” this variable is also a product of experiments. A linear function was formulated from a set of experiments to decide the most effective size of object to remove from the image considering maximum removal of noise and minimum removal of nanoparticles objects:

(10)SmallestObjectToRemove=-26×img_res+2033;

Code (10) is the linear function of the variable “SmallestObjectToRemove”. The value “img_res” is given by the user at the beginning of the program and it represents the value of the scale bar in nanometers. By transforming the noise removal dynamic is it possible to process images at different magnifications without the loss of data.

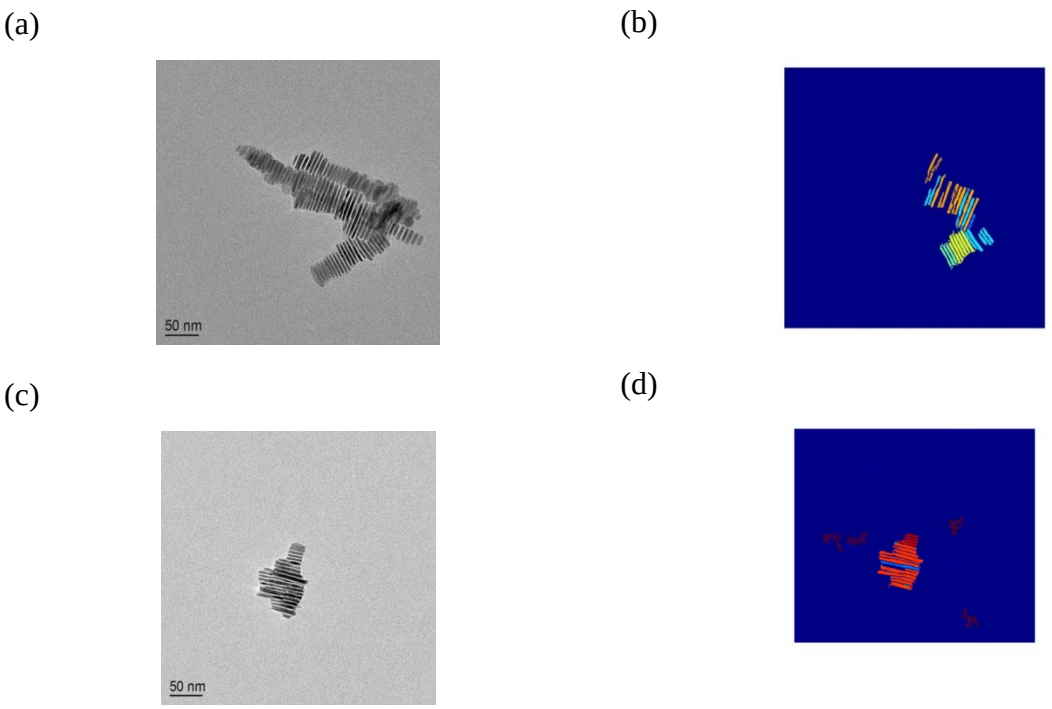

Figure 4.1: *Two examples out of many images used pre and post fully automation program run . (a&b) BF TEM original images as taken from the T-12. (c)The outcome of the image (a). A color map presenting the “angleofScan” variable, the lower arrays represent a good example of the necessity of the shifting angle as a single arrays is composed of three different colors. (d) The outcome of image (b).In this image a short order background noise had passed the noise removal algorithm. These noise objects are dealt statistically.*

The program was executed on tens of TEM images generating a database of 1292 objects each hold a major and minor axes lengths. Figure 4.1 represents two images sampled from the database. The outcome of Figure 4.1a is Figure 4.1b. In this image the importance of the angles scan can be clearly observed as the lower arrays is shown by the varying colors of each angle that builds it. Figure 4.1d is the output of Figure 4.1c. In this image it is possible to observe several short order background noises. This noise is filtered in the statistical chapter and is created due to tradeoff between removal of noise and maintaining the nanoparticles.

Summary of the program is presented in the following flowchart:

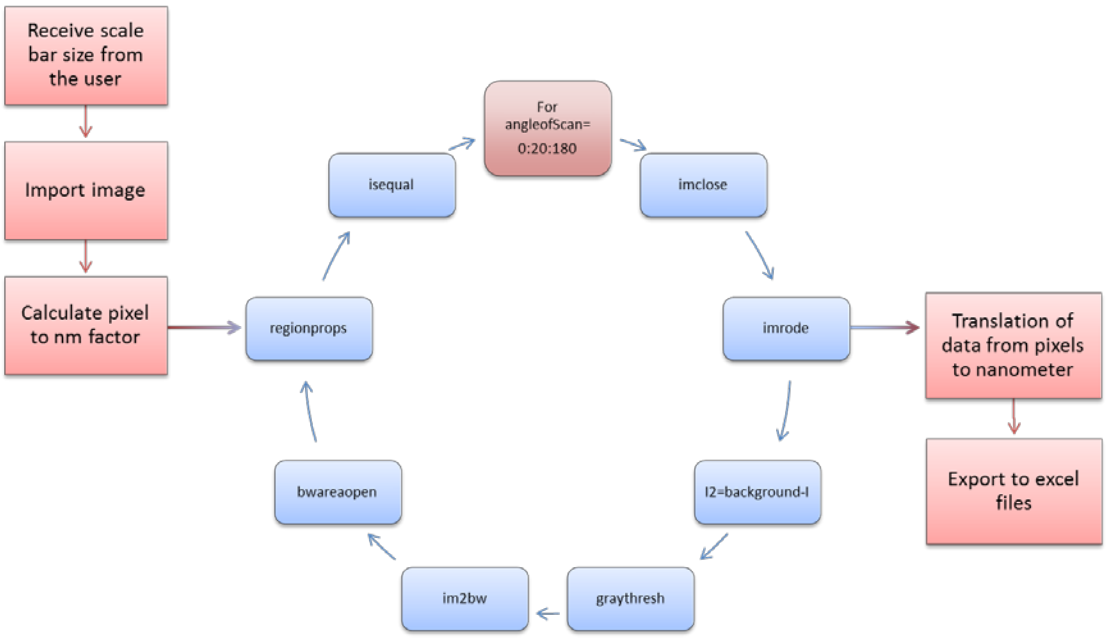

Figure 4.2: *Summarized flowchart of the program.*

5 Statistics

The 1292 object containing the major and minor axes lengths were statistically quantified using the software “Statistica”. In addition, a single image was taken for intense investigation.

5.1 Quantitative Statistics

At first, the background noise which can be seen in Figure 4.1d was removed by practical observation in Figure 5.1. Observation of Figure 5.1a reveals that may of the objects cannot be real CuS nanoparticles plates as the minor axis length is longer or not reasonably short enough to present a nanoplate. This argument is strengthened by Figure 5.1b. Figure 5.1b presents two objects populations. The upper left is expected to be the data of the nanoplates as the Major axis length is longer than the minor unlike the lower right group with the opposite properties. As a result of the initial data analysis a removal of all objects with a ratio of 4 to 1 and below between the major to the minor axis was decided. This decision reduced the objects database to 670 items.

(a) (b)

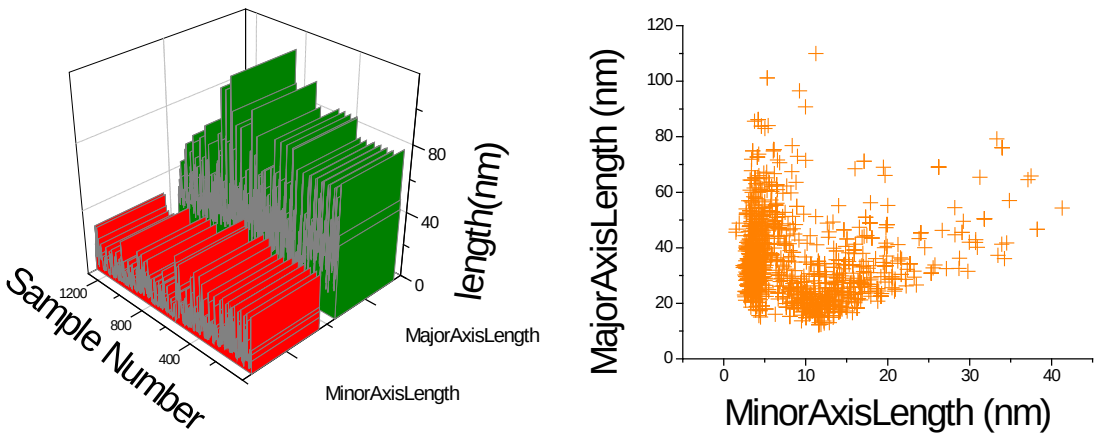

Figure 5.1: *origin generated raw data of the 1292 objects holding major asix and minor axis lengths. (a) a 3D ribbons graph showing the ratio between the major and minor axis length of each object. (b) A 2D scatter praph that present two main populations of object with inverted size ratios.*

Afterwards, Histograms of each Axis were generated and the statistical data was extracted as can be seen in Figure 5.2.

(a) (b)

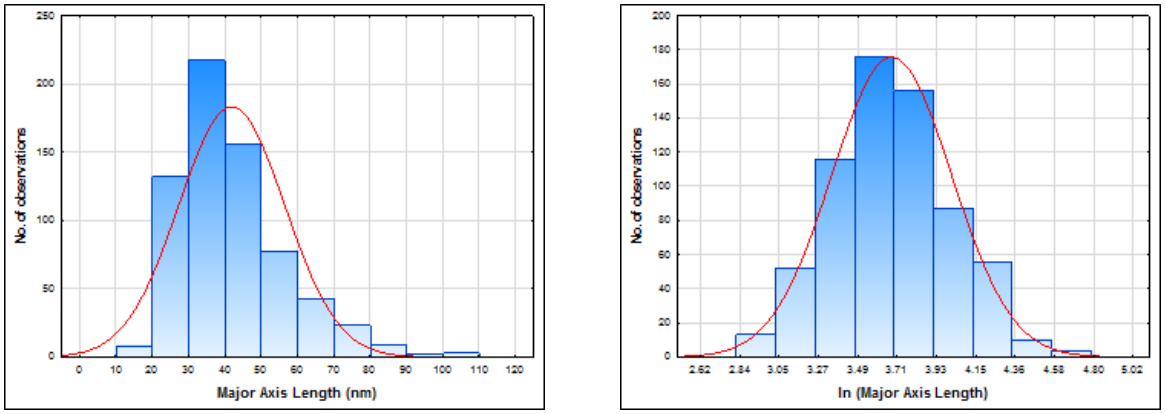

(c) (d)

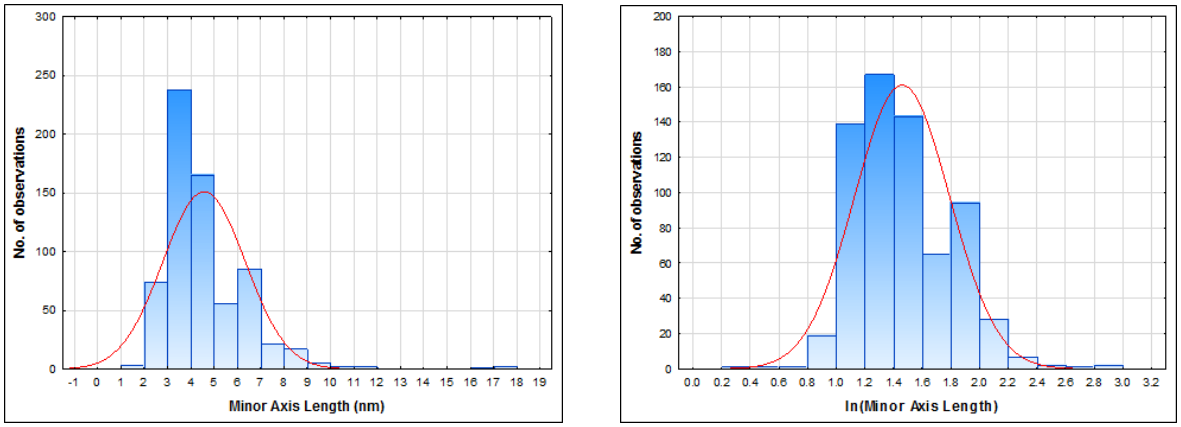

Figure 5.2: *Length histogram of the 670 objects in the database. (a) Major axis length histogram. (b)lan transformation of the major axis length histogram. (c) Minor axis length histogram. (d)lan transformation of the major axis length histogram.*

Figure 5.2a and Figure 5.2c presents the major and minor axes histograms. Both histograms have distribution imperfections. In Figure 5.2a a tail of long particles was found. This result is reasonable as there is no absolute control over the synthesis and occasionally some nanoparticles grow beyond the average size. Figure 5.2c shows two populations of particles. The Main population length is 3-4 nm and the minor population length is 6-7 nm. Similarly, to the major axis data two population is a reasonable result in nanoparticles synthesis. In order to improve the distribution of the population lan transformation of all values was conducted. This action is common in statistical science for amplification of the major populations in the database. Figure 5.2b and Figure 5.2d presents the lan transformation of the major and minor axes histograms. An improvement of the distribution can be observed in both histograms and from it the major populations can be visually detected.

Table 5.1: *Summery of Output data extracted from the objects histograms*

	Mean	Median	Minimum	Maximum	Variance	Std.Dev.
Major axis	41.93	39.26	17.60	109.97	213.52	14.61
Minor axis	4.57	4.11	1.48	17.12	3.14	1.77

Table 5.1 presents the output of the objects histograms in Figure 5.2a and Figure 5.2c. In addition, a function can be constructed from combination of the two histograms as can be seen in Figure 5.3.

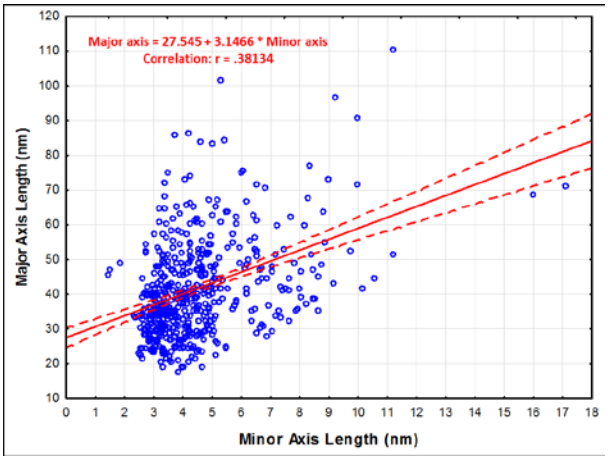

Figure 5.3: *Major vs. Minor function extracted from the axis's histograms.*

The linear fit of the scatterplot in Figure 5.3 produced a function that can correlate between the two axes at a reliability of r=0.38. Observation of the r function in Figure 5.3 can provide additional understanding of the error. It can be seen that the error increases dramatically as function of the distance to ~4.5nm. Thus, in the range of $4.5nm \pm 2nm$ the function prediction can be trusted.

5.2 Manual Comparison

Unlike the previous chapter that deals with a large database, the extraction of the data and its reliability, this chapter discuss the value of the program when compared to manual counting. Figure 5.4 presents a randomly chosen image for the comparison of methods.

(a) (b)

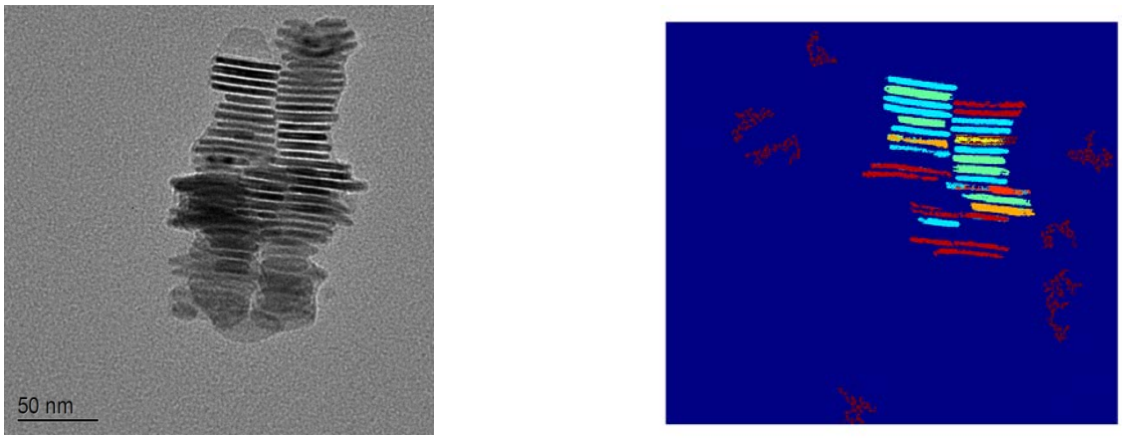

Figure 5.4: *the image used for manual to automatic comparison. (a) BF TEM original image as taken from the T-12. (d) The outcome of image process.*

The major the minor axes lengths were extracted from Figure 5.4a both by the program and by manual measurements conducted using DigitalMicrograph. Figure 5.5 present a box & whisker graphs of the data.

(a) (b)

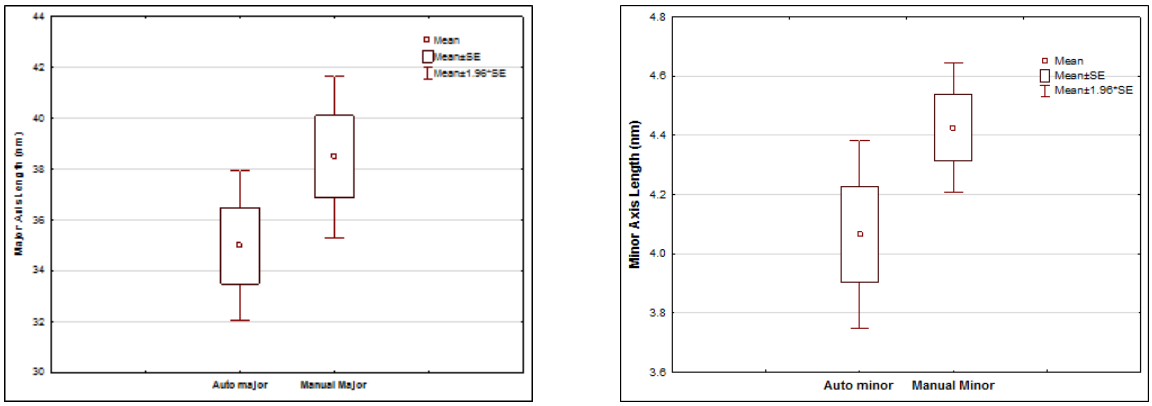

Figure 5.5: *Box & Whisker Graph of Automatic and manual size measurements. (a) Major axis graph. (b) Minor axis graph.*

The data presented in Figure 5.5 was summarized in Table 5.2.

Table 5.2: *Summery of Output data extracted from the box & whisker graphs*

	Mean Automatic	Mean Manual	%Difference	Std.Dev. Automatic	Std.Dev. Manual
Automatic major vs. Manual Major	34.98	38.48	10.03	7.66	6.30
Automatic minor vs. Manual Minor	4.06	4.43	8.89	0.83	0.43

Assuming that the manual measurements are more accurate than the automatic an error of lower values can be observed for both axes. This error is expected due to the fact that the CuS nanoparticles are coated with surfactants. The surfactant is brighter that the nanoparticle and

cannot be detected by the program algorithm. In summary, the difference is 10.03% or lower between the automatic to the manual measurement, In addition, the difference is constant which means that the ratio of the nanoparticles is maintained. This outcome has tremendous importance as the surface plasmon resonance is more sensitive to axes size ratio than the actual size in this error range.

6 Conclusions

- The System is not perfect. Image Processing software are complicated and complex software to program. This work presents an idea of creating and programing a new algorithm designed of a specific target and by doing so provide a proof of concept.
- Writing a designated code for a specific problem produce reliable results and more important it allow the freedom of improvement and access of the source of the algorithm.

7 References

1. Wu, C.; Yu, S.-H.; Antonietti, M., Complex concaved cuboctahedrons of copper sulfide crystals with highly geometrical symmetry created by a solution process. *Chem. Mater.* 2006, 18, 3599-3601.
2. Wu, C.; Yu, S.-H.; Chen, S.; Liu, G.; Liu, B., Large scale synthesis of uniform CuS nanotubes in ethylene glycol by a sacrificial templating method under mild conditions. *J. Mater. Chem.* 2006, 16, 3326-3331.
3. Zhang, H. T.; Wu, G.; Chen, X. H., Controlled synthesis and characterization of covellite (CuS) nanoflakes. *Mater. Chem. Phys.* 2006, 98, 298-303.
4. Goncalves, A. P.; Lopes, E. B.; Casaca, A.; Dias, M.; Almeida, M., Growth of CuS platelet single crystals by the high-temperature solution growth technique. *J. Cryst. Growth* 2008, 310, 2742-2745.
5. Zhang, F.; Wong, S. S., Controlled Synthesis of Semiconducting Metal Sulfide Nanowires. *Chem. Mater.* 2009, 21, 4541-4554.
6. Salavati-Niasari, M.; Alizadeh, S.; Mousavi-Kamazani, M.; Mir, N.; Rezaei, O.; Ahmadi, E., Surfactant-Free Fabrication of Copper Sulfides (CuS, Cu2S) via Hydrothermal Method. *J. Clust. Sci.* 2013, 24, 1181-1191.
7. Wang, S.; Ning, J.; Zhao, L.; Liu, B.; Zou, B., Facile synthesis and assembly of CuS nano-flakes to novel hexagonal prism structures. *J. Cryst. Growth* 2010, 312, 2060-2064.
8. Li, B.; Xie, Y.; Xue, Y., Controllable Synthesis of CuS Nanostructures from Self-Assembled Precursors with Biomolecule Assistance. *J. Phys. Chem. C* 2007, 111, 12181-12187.
9. Du, W.; Qian, X.; Ma, X.; Gong, Q.; Cao, H.; Yin, J., Shape-controlled synthesis and self-assembly of hexagonal covellite (CuS) nanoplatelets. *Chem. - Eur. J.* 2007, 13, 3241-3247.
10. Saunders, A. E.; Ghezelbash, A.; Smilgies, D.-M.; Sigman, M. B., Jr.; Korgel, B. A., Columnar Self-Assembly of Colloidal Nanodisks. *Nano Lett.* 2006, 6, 2959-2963.

11. Qin, A.-M.; Fang, Y.-P.; Ou, H.-D.; Liu, H.-Q.; Su, C.-Y., Formation of Various Morphologies of Covellite Copper Sulfide Submicron Crystals by a Hydrothermal Method without Surfactant. *Cryst. Growth Des.* 2005, 5, 855-860.
12. Ghezelbash, A.; Korgel, B. A., Nickel Sulfide and Copper Sulfide Nanocrystal Synthesis and Polymorphism. *Langmuir* 2005, 21, 9451-9456.
13. Pradhan, N.; Katz, B.; Efrima, S., Synthesis of High-Quality Metal Sulfide Nanoparticles from Alkyl Xanthate Single Precursors in Alkylamine Solvents. *J. Phys. Chem. B* 2003, 107, 13843-13854.
14. Larsen, T. H.; Sigman, M.; Ghezelbash, A.; Doty, R. C.; Korgel, B. A., Solventless Synthesis of Copper Sulfide Nanorods by Thermolysis of a Single Source Thiolate-Derived Precursor. *J. Am. Chem. Soc.* 2003, 125, 5638-5639.
15. Basu, M.; Sinha, A. K.; Pradhan, M.; Sarkar, S.; Negishi, Y.; Govind; Pal, T., Evolution of Hierarchical Hexagonal Stacked Plates of CuS from Liquid-Liquid Interface and its Photocatalytic Application for Oxidative Degradation of Different Dyes under Indoor Lighting. *Environ. Sci. Technol.* 2010, 44, 6313-6318.
16. Mukherjee, N.; Sinha, A.; Khan, G. G.; Chandra, D.; Bhaumik, A.; Mondal, A., A study on the structural and mechanical properties of nanocrystalline CuS thin films grown by chemical bath deposition technique. *Mater. Res. Bull.* 2011, 46, 6-11.
17. Liufu, S.-C.; Chen, L.-D.; Yao, Q.; Huang, F.-Q., In Situ Assembly of CuxS Quantum-Dots into Thin Film: A Highly Conductive P-Type Transparent Film. *J. Phys. Chem. C* 2008, 112, 12085-12088.
18. Zia, R.; Schuller, J. A.; Chandran, A.; Brongersma, M. L., Plasmonics: the next chip-scale technology. *Mater. Today (Oxford, U. K.)* 2006, 9, 20-27.
19. Schuller, J. A.; Barnard, E. S.; Cai, W.; Jun, Y. C.; White, J. S.; Brongersma, M. L., Plasmonics for extreme light concentration and manipulation. *Nat Mater* 2010, 9, 193-204.
20. Hsu, S.-W.; On, K.; Tao, A. R., Localized Surface Plasmon Resonances of Anisotropic Semiconductor Nanocrystals. *J. Am. Chem. Soc.* 2011, 133, 19072-19075.
21. Petryayeva, E.; Krull, U. J., Localized surface plasmon resonance: Nanostructures, bioassays and biosensing—A review. *Analytica Chimica Acta* 2011, 706, 8-24.
22. Wei, T.; Liu, Y.; Dong, W.; Zhang, Y.; Huang, C.; Sun, Y.; Chen, X.; Dai, N., Surface-Dependent Localized Surface Plasmon Resonances in CuS Nanodisks. *ACS Applied Materials & Interfaces* 2013, 5, 10473-10477.
23. Morales-Garcia, A.; Soares, A. L., Jr.; Dos Santos, E. C.; de Abreu, H. A.; Duarte, H. A., First-principles calculations and electron density topological analysis of covellite (CuS). *The journal of physical chemistry. A* 2014, 118, 5823-31.
24. Saito, S.-h.; Kishi, H.; Nie, K.; Nakamaru, H.; Wagatsuma, F.; Shinohara, T., 63Cu NMR studies of copper sulfide. *Phys. Rev. B: Condens. Matter* 1997, 55, 14527-14535.
25. Liang, W.; Whangbo, M. H., Conductivity anisotropy and structural phase transition in covellite CuS. *Solid State Commun.* 1993, 85, 405-8.
26. Nozaki, H.; Shibata, K.; Ohhashi, N., Metallic hole conduction in CuS. *Journal. Solid State Chemistry* 1991, 91, 306-311.
27. Otsu, N., A threshold selection method from gray-level histograms. *Automatica* 1979, 11, 23-27.